Available online at www.sciencedirect.com
SCIENCE DIRECT®
Journal of Power Sources 128 (2004) 193–200
JOURNAL OF POWER SOURCES
www.elsevier.com/locate/jpowsour

Ferritic stainless steels as bipolar plate material for polymer electrolyte membrane fuel cells

Heli Wang, John A. Turner*

National Renewable Energy Laboratory, 1617 Cole Blvd., Golden, CO 80401, USA

Received 5 September 2003; accepted 26 September 2003

Abstract

Both interfacial contact resistance (ICR) measurements and electrochemical corrosion techniques were applied to ferritic stainless steels in a solution simulating the environment of a bipolar plate in a polymer electrolyte membrane fuel cell (PEMFC). Stainless steel samples of AISI434, AISI436, AISI441, AISI444, and AISI446 were studied, and the results suggest that AISI446 could be considered as a candidate bipolar plate material. In both polymer electrolyte membrane fuel cell anode and cathode environments, AISI446 steel underwent passivation and the passive films were very stable. An increase in the ICR between the steel and the carbon backing material due to the passive film formation was noted. The thickness of the passive film on AISI446 was estimated to be 2.6 nm for the film formed at −0.1 V in the simulated PEMFC anode environment and 3.0 nm for the film formed at 0.6 V in the simulated PEMFC cathode environment. Further improvement in the ICR will require some modification of the passive film, which is dominated by chromium oxide.

Keywords: Bipolar plate; Stainless steel; Ferrite; PEMFC; Passive film

1. Introduction

The polymer electrolyte membrane fuel cell (PEMFC) is a clean energy system that can convert hydrogen and oxygen (or air) directly to electricity with water as the only chemical by-product [1]. The hydrogen oxidation reaction occurs in the PEMFC anode side, while the oxygen reduction reaction occurs in the PEMFC cathode side. Since a single cell can only give an output voltage of around 0.5–0.7 V the cells are stacked together in series, connected by means of bipolar plates. The combination of the size of the plates (relating to the total current), coupled to the number of cells in the stack, provides the requisite power.

The bipolar plates are a multifunctional component in this stack as they provide electrical continuity between the cells, they separate the gasses, and the flow channels in the plates deliver the reacting gasses to the fuel cell electrodes. Classic fuel cell stacks used graphite material as the bipolar plate; while its properties are ideal, its high cost, and the need for machining to form the flow channels, eliminate this material for applications involving high-volume manufacturing. Alternatives that have been investigated as bipolar plate material include: carbon composite material [2,3], coated metals [4,5], and Fe-based alloys and stainless steels [6–12]. Stainless steel materials have received considerable attention due to their relatively high strength, high chemical stability, low gas permeability, wide range of alloy choice, and applicability to mass production, as well as cost considerations [1]. In addition, using thin sheets can compensate for the high material density, and stainless steel screen has been proposed [13,14] to remove the cost of forming flow-fields on the metals.

Most of the work on stainless steel bipolar plate material has been on the austenitic stainless steels [7,8,10,11]. Previous investigations in our laboratory looking at a variety of alloys showed that 349™ stainless steel exhibited superior behavior in a simulated PEMFC environment and would be an excellent candidate material for bipolar plates [15]. In that work, it was observed that the performance depended on the amount of chromium in the alloy, with higher chromium leading to better properties. However, these alloys also have a high nickel component, which increases their cost, leading one to evaluate lower-cost alloys. Our earlier work on the nature of the passive film with these materials showed that nickel is not a major component in the oxide film [16], indicating that perhaps nickel could be eliminated without changing the performance. In addition, recent work has shown that nickel from 316 L stainless steel can be a

* Corresponding author. Tel.: +1-303-275-4270; fax: +1-303-275-3033.
E-mail address: john_turner@nrel.gov (J.A. Turner).

0378-7753/$ – see front matter © 2003 Elsevier B.V. All rights reserved.
doi:10.1016/j.jpowsour.2003.09.075

major containment in the membrane, reducing overall conductivity [17]. Thus far, there has been very little work with the ferrite stainless steels [18], which have little or no nickel component but have similar amounts of chromium. A selection of these materials was therefore chosen for this report.

2. Experimental

2.1. Materials and electrochemistry

Ferrite stainless steels samples of AISI434, AISI436, AISI441, AISI444, and AISI446 were provided by J & L Specialty Steel, Inc. Their chemical compositions are given in Table 1. The plates were cut into samples of 2.54 cm × 1.25 cm, polished with #600 grit SiC abrasive paper, rinsed with acetone, and dried with nitrogen gas. An electrical contact was made to one side by means of silver paint. Then the contact side (backside) and the edges of the samples were covered with an insulating epoxy, leaving one side for electrochemical measurements. The sealing process was repeated to eliminate possible leakage.

To simulate direct contact with the membrane (worst case for corrosion) and an aggressive PEMFC environment, all electrochemical experiments were conducted in 1 M H_2SO_4 + 2 ppm F^- solution at 70 °C [12,19]. The solution was bubbled thoroughly either with hydrogen gas (for a simulated PEMFC anode environment) or pressurized air (for a simulated PEMFC cathode environment) prior to and during the electrochemical measurements.

A conventional three-electrode system was used for the electrochemical measurements, with a platinum sheet as the counter electrode and a saturated calomel electrode (SCE) as the reference electrode. Unless otherwise specified, all electrode potentials will be referenced to the SCE. A Solartron 1287 potentiostat interfaced with a computer controlled the electrochemical experiments. Dynamic polarization was used to compare the general corrosion resistance of the steels. In these tests, samples were stabilized at the open circuit potential (OCP) for 5 min, and then the potential was swept from the OCP towards anodic potentials with a scanning rate of 1 mV/s.

To investigate the performance and the stability of these steels under PEMFCs' operation conditions, potentiostatic polarization experiments were conducted. In these measurements, samples were also stabilized at OCP for 5 min then a specific potential was applied and the current-time curves were recorded. Two potentials were chosen for the tests: for the fuel cell anode condition, −0.1 V (equivalent to ∼0.1 V_{NHE}) was used, with the solution sparged with hydrogen gas, and for the cathode condition, 0.6 V (equivalent to ∼0.8 V_{NHE}) was used with the solution sparged with air [19].

2.2. Interfacial contact resistance (ICR)

All ICR measurements were carried out at room temperature with dry samples. The method for conducting ICR measurements has been previously described [15]. In short, two pieces of conductive carbon papers were sandwiched between the stainless steel sample and the two copper plates. A current of 1.000 A was provided via the two copper plates and the total voltage drop was registered as a function of the gradually increasing compaction force. The total resistance dependency on the compaction force could then be calculated. To eliminate the possible interference from the oxide layer on the copper plates, the plates were polished mechanically before the measurement and a calibration was carried out. Similarly, the ICR value of the carbon paper/copper plate interface ($R_{C/Cu}$) was corrected by a calibration [15]. Therefore, this report gives only the corrected ICR values for the carbon paper/stainless steel interface for the air-formed film $R_{C/SS}$ or the passive film $R_{C/PF}$).

Two types of surface films on the stainless steel samples were investigated. The first group consisted of fresh samples of the different grades. They were polished with #600 SiC paper, rinsed with acetone then dried with nitrogen gas. At this point, the surface of the ferrite steel is covered only with a naturally occurring air-formed oxide film. The second group consisted of samples of the candidate steels that were pre-polarized at specific potentials. In these measurements the steel samples were potentiostatically polarized in the solution forming a passive film due to the polarisation. They were then un-sealed and the sealed side (backside) was polished to #600 SiC abrasive paper followed by rinsing with acetone and drying with pressurized nitrogen gas. Thus, the backside of the steel sample would be covered only with an air-formed film. The ICR values $R_{C/SS}$ from the previous measurements can then be used to do the correction, giving only the $R_{C/PF}$ component.

Table 1
Chemical compositions of the stainless steel samples

Grade	Cr	Ni	Mn	Si	Mo	Other[a]	Fe
AISI434	17.946	–	0.289	0.285	0.938		Balance
AISI436	18.101	–	0.505	0.370	1.037	Cb0.3, Ti0.2	Balance
AISI441	18.230	–	0.519	0.506	0.033	Cb0.69, Ti0.27	Balance
AISI444	18.485	–	0.186	0.382	1.763	Ti + Cb ≤ 0.80	Balance
AISI446	28.367	2.958	0.434	0.424	3.502	Ti + Cb ≤ 0.75	Balance

[a] From the website of J & L Specialty Steels, Inc.

2.3. X-ray photoelectron spectroscopy (XPS)

In order to identify the influence of polarization on the chemical composition of the surface passive film, the surfaces of non-polarized and polarized samples were investigated via XPS. The procedure for the XPS experiments has been described elsewhere [16]. In short, the XPS analysis was carried out in a Phi 5600 electron spectrometer using Al Kα radiation X-ray source (1486.6 eV) and a hemispherical energy analyzer. The base pressure in the spectrometer chamber was 1.33×10^{-8} Pa. The depth profiles were obtained by means of sputtering with 3 keV argon ions. During the sputtering, the argon pressure in the chamber was 6.67×10^{-5} Pa. To estimate the sputtering rate, a thin Nb-oxide film was sputtered all the way through and it was found that the sputtering rate was about 20 Å/min. Due to the roughness of the sample surface, the XPS analysis could only give qualitative analysis about the films.

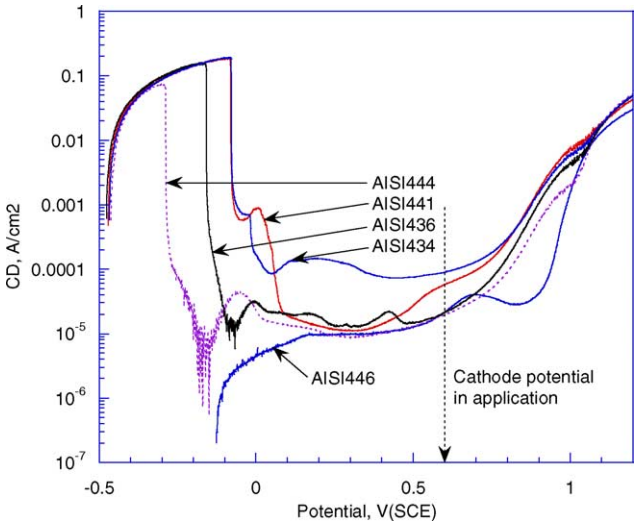

Fig. 2. Anodic behavior of stainless steels in 1 M H_2SO_4 + 2 ppm F^- at 70 °C purged with air. The cathode potential in PEMFCs application is marked.

3. Results and discussion

3.1. Polarization behavior of stainless steels

Figs. 1 and 2 give the anodic polarization curves for the different stainless steels in 1 M H_2SO_4 + 2 ppm F^- at 70 °C, note that all of the investigated steels show passivation behavior. Fig. 1 gives the results when the solution was purged with hydrogen. The operating potential for the PEMFC's anode condition, (approximately −0.1 V according to [19]), is marked in the figure. It is apparent that this potential is in the passive region for all the materials tested. Fig. 2 shows the results when the solution was purged with pressurized air. Similarly, the operating potential for the PEMFC's cathode condition (around 0.6 V), is also marked in the figure. Again, this cathode potential is in the passive region for all the materials tested.

Based on these results, the five tested steels can be paired as: AISI434/AISI441, AISI436/AISI444, and AISI446 alone. Both AISI434 and AISI441 showed a passivation at −0.15 V when the solution was purged with hydrogen gas (Fig. 1) and at −0.08 V when the solution was purged with air (Fig. 2). However, a very high critical current (the peak current for passivation) of over 0.1 A/cm^2 was recorded for these two steels under both conditions. An additional current peak was observed at around 0.02 V in the hydrogen-purged solution and at −0.02 to 0 V in the

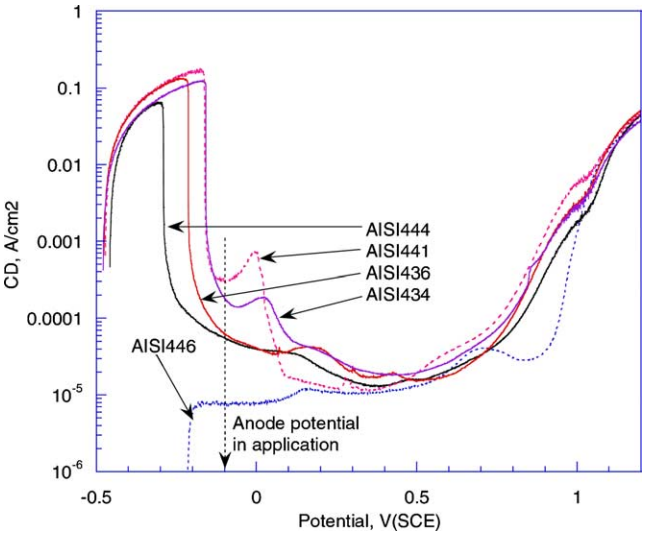

Fig. 1. Anodic behavior of stainless steels in 1 M H_2SO_4 + 2 ppm F^- at 70 °C purged with H_2. The anode potential in a PEMFCs environment is marked.

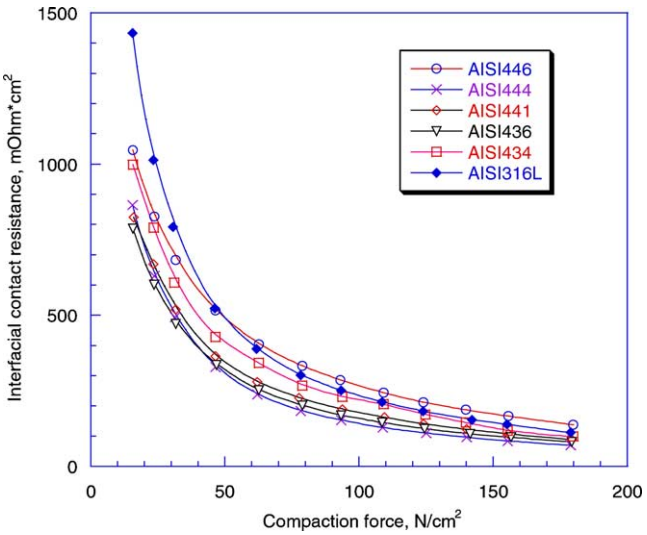

Fig. 3. Interfacial contact resistances for different stainless steels and carbon paper as a function of compaction forces. ICR for S316L is shown for reference.

air-purged solution, followed by the normal passivation. The reason for this second peak is yet unclear. In addition, the current density at −0.1 V in PEMFC anode condition (i_{anode}) is 200 μA/cm^2 for AISI434 and 300 μA/cm^2 for AISI441; while the current density at 0.6 V in PEMFC cathode condition ($i_{cathode}$) is 100 μA/cm^2 for AISI434 and 60 μA/cm^2 for AISI441. These high passivation current densities and the high critical current values preclude these steels from being used as is in a fuel cell environment.

Polarization curves for AISI436 and AISI444 are very much similar, with AISI444 showing a wider passivation region than AISI436 in both conditions. The critical current for AISI436 is still very high, over 0.1 A/cm^2 under both PEMFC anode and cathode conditions. The critical current for AISI441 is a little lower than that for AISI436, but still over 60 mA/cm^2 under both anode and cathode conditions. Moreover, i_{anode} is over 60 μA/cm^2 for AISI436 and over 50 μA/cm^2 for AISI444; $i_{cathode}$ is around 20 μA/cm^2 for both AISI436 and AISI444. Even though the $i_{cathode}$ level is reduced significantly, the high critical current and the high level of i_{anode} indicate that neither AISI436 nor AISI444 steel are viable materials for fuel cell environments.

On the other hand, AISI446 has a much wider passivation region than the others. The passivation current, which is the lowest current in the passivation region, is around 10–15 μA/cm^2 for AISI446 under both conditions. In the simulated anode environment, i_{anode} is around 8 μA/cm^2 for AISI446 (Fig. 1). In the simulated PEMFC cathode environment, $i_{cathode}$ is around 20 μA/cm^2 for AISI446 (Fig. 2). With these current densities, it is reasonable to consider AISI446 as a candidate material for bipolar plates.

The behavior of the ferrite stainless steels in simulated PEMFC environments may be related to Cr in the alloy as the primary passivating element [20–22]. In general, the current density at the operating condition decreases with an increase of the chromium content in the alloy. This is similar to the behavior reported for the austenite stainless steels [15]. However, this relationship is not strictly followed for the AISI400 series steels. The reason is likely due to other alloying elements like Ni and Mo that have their own contribution to the passivation and the nature of passive film in these environments. In particular, the similarity of the anodic behavior of AISI434 and AISI441 indicates that the trace elements have the same or even a greater influence as 1% Mo, since the passivation current was reduced significantly with the addition of Cb and Ti as trace metals. The additional influence of Mo can also be seen from the curves of AISI436 and AISI444. The higher Mo content gave a wider passivation region. With the exception of AISI446, the ferrite stainless steels in this study have ∼18% Cr content; AISI446 has a very high Cr content of 28%. Therefore, the significant difference in the anodic performance of AISI446 is likely to be related directly to the high Cr concentration. Additionally, we note that AISI446 has Ni at ∼3% and Mo at ∼3.5% which may also have some bearing on its behavior; detailed research is needed to understand the influence of the additional alloying elements.

Careful inspection of Figs. 1 and 2, show that there is a broad peak at approximately 0.7 V for AISI446 in both the figures. Similar behavior has been reported for AISI310 stainless steel [23]. This peak has been identified as due to the oxidation of Cr_2O_3 in the passive film to a higher valance state [23–25]. The higher Cr content of AISI446 among the steels tested appears to be the reason that only AISI446 exhibited this behavior.

Considering the polarization results only, in the PEMFC anode environment, the materials' performance is in the order of AISI446 > AISI444 > AISI436 > AISI434 > AISI441. For the cathode environment, the materials are in the order of AISI446 > AISI444 ≥ AISI436 > AISI441 > AISI434. Both of the above orders suggest that AISI446 is the best candidate among the materials tested. Obviously, more investigations are warranted with this steel.

3.2. Interfacial contact resistance

The interfacial contact resistance with the fresh stainless steel samples and carbon paper was determined for different compaction forces, Fig. 3. Note, only one interface for the carbon paper/surface film formed in air ($R_{C/SS}$) is plotted. For comparison, Fig. 3 also gives the ICR values for AISI316L stainless steel obtained under the same conditions. At a compaction force of 140 N/cm^2, the interfacial contact resistance is in the order of 100–200 mΩ cm^2 for all the steels tested. It can be seen that the performance of most of the samples has the same general behavior as that of AISI316L, but with lower ICR values than those of AISI316L. The exception is AISI446, which is slightly higher than AISI316L. The ICR results give the performance order of: AISI444 > AISI436 > AISI441 > AISI434 > AISI446. This is almost the same as the electrochemical performance order except for AISI446. However, in comparison to previous measurements [6–11], AISI446 is still an excellent candidate material for PEMFC bipolar plates since the differences in ICR values are rather small. Therefore, further measurements were carried out in simulated PEMFC anode and cathode environments with AISI446.

From Figs. 1 and 2, we see that the surface of AISI446 steel can easily be passivated under the PEMFC environment. The major concern would then be the affect of the passive film formed under operating conditions would have on the contact resistance. To this end, the ICR value was checked both for AISI446 samples polarized at 0.6 V in simulated PEMFC cathode environment, and for samples polarized at −0.1 V in simulated PEMFC anode environment. The results for samples pre-treated under potentiostatic conditions for 7.5 h in both environments are shown in Fig. 4. For comparison purpose, results from fresh samples are plotted again in Fig. 4. In general, passivation has a significant influence on the ICR value. After passivation, the ICR values for AISI446 steel increase, regardless the PEMFC

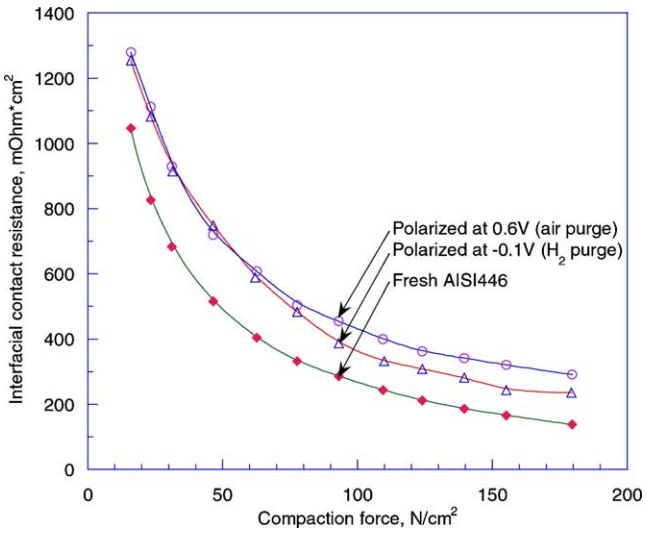

Fig. 4. Effect of passivation on the interfacial contact resistance between the passive film and carbon paper.

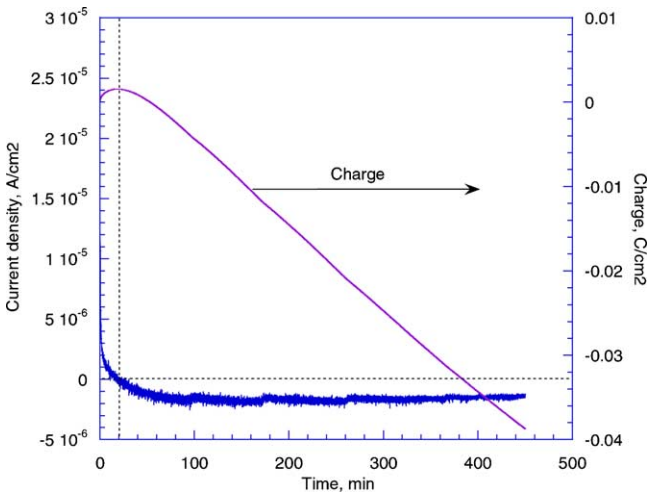

Fig. 5. Transient current and accumulated charge of AISI446 stainless steel at −0.1 V in 1 M H_2SO_4 + 2 ppm F^- at 70 °C purged with hydrogen gas.

environment. Similar behavior was noted for 349™ stainless steel [15]. This shift in ICR values is due to the fact that the nature and composition of the passive film is different from the air-formed oxide film. It is also noted that the steel has a slightly higher ICR value when it is polarized at 0.6 V in air-purged solution than when it is polarized at −0.1 V in a hydrogen gas-purged one. This is in agreement with the general understanding that oxidation of the steel surface is easier in air-purged solution than in hydrogen gas-purged one. So, one may expect a thicker passive film when the steel is treated in air-purged environment than that treated in the hydrogen environment. The ICR value at 140 N/cm^2 is approximately 350 mΩ cm^2 for sample polarized at 0.6 V in simulated PEMFC cathode environment, and approximately 280 mΩ cm^2 for sample polarized at −0.1 V in simulated PEMFC anode environment, both of which are higher than those for 349™ treated under the same conditions [15] and may be too high for use as a bipolar plate in a fuel cell stack.

3.3. Potentiostatic polarization for AISI446

Hydrogen oxidation is the anode reaction in PEMFCs. So, the major concern for the material in this environment would be its anti-corrosion behavior and the film stability. It can be seen from Fig. 1 that the operating anode potential of around −0.1 V is close to the open circuit potential for AISI446 in 1 M H_2SO_4 + 2 ppm F^- solution at 70 °C. Since the steel may undergo dissolution at this potential, potentiostatic measurements for AISI446 samples in solution purged with hydrogen gas were conducted at −0.1 V. The current-time behavior is shown in Fig. 5.

From Fig. 5, it is noted that the transient current decays very fast at the beginning of polarization; then the current stabilizes. Similar results were reported for 349™ stainless steel [15] and AISI316L stainless steel in a pH 1 solution at 80 °C [18]. The fast decay of the current is related to the passive film formation process. As soon as the whole surface is covered with the passive film, the current needed to maintain the passivation should be very low. After approximately 20 min at −0.1 V, the current undergoes a positive–negative transition. The accumulated charge curve in Fig. 5 gives a better view concerning this transition, which occurs when the accumulated charge is in its maximum, as marked in Fig. 5. A similar current transition was observed for 349™ steel [15]. However, this is different from previous investigations with other austenite stainless steels where only anodic current was expressed [12,26] indicating a low continuous dissolution of the surface film. The reason for the cathodic current is not yet clear. However, a cathodic (negative) current here indicates that the as-formed

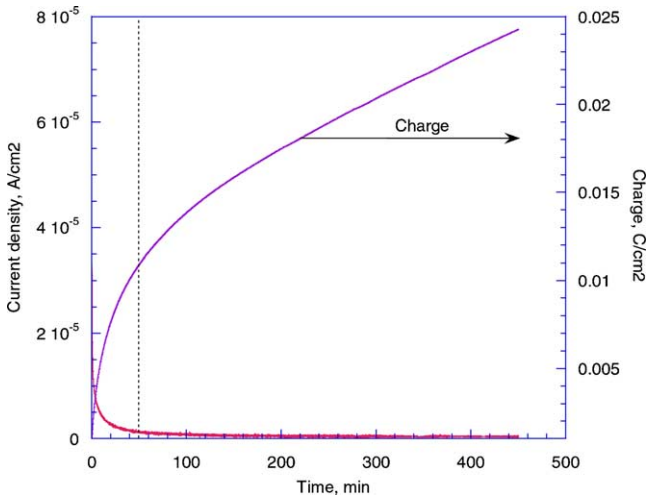

Fig. 6. Transient current and accumulated charge of AISI446 stainless steel at 0.6 V in 1 M H_2SO_4 + 2 ppm F^- at 70 °C purged with pressurized air.

passive film is cathodically protected, so there would not be active dissolution of the film under this condition. The above results suggest that the anodic dissolution of the material in simulated PEMFC anode environment could be prevented after the passive film is formed. From Fig. 5 it is seen that the current curve is relatively steady in the range of 1–2 $\mu A/cm^2$ during the test period giving rise to the linear charge–time relationship as shown. All this indicates that the passive film is stable under these conditions.

Oxygen reduction is the cathode reaction in PEMFCs and the environment is oxidative. Potentiostatic measurements were carried out at 0.6 V in solution purged with air; the passivation behavior is shown in Fig. 6. The trends in Figs. 5 and 6 are identical. Similarly, passivation occurred rapidly with a fast current decay, and then the current stabilized and remained at a very low level of 0.3–1.0 $\mu A/cm^2$. Moreover, the current curve in Fig. 6 indicates that the passive film is very stable under the cathode environment. Comparing Fig. 6 with Fig. 5, it is seen that the current does not have an anodic to cathodic transition; the current is always anodic. This might be related to fact that the applied potential is in the middle of the passivation region. Fig. 6 also shows the accumulated charge used for the passivation. It is noticed that there is a fast increase of charge in the beginning of passivation, followed by a linear charge–time relation. This linear charge–time relationship clearly indicates that the anodic current is very stable during the measurement period. It is also noted that for this material, the time needed for the current to stabilize in PEMFC cathode environment is longer than that in PEMFC anode environment, possibly due to either a thicker passive film formation or a different passive film composition. Referring to Fig. 6, it is seen that approximately 50 min is needed before the film stabilizes and a linear charge–time relationship is reached.

3.4. XPS depth profile

Figs. 7 and 8 give the XPS depth profiles for AISI446 with an air-formed oxide film and with passive films formed from polarization in simulated PEMFC environments, respectively. The air-formed film is composed of iron oxides and chromium oxide, Fig. 7, with a Fe-rich outer layer and a Cr-rich inner layer. The depth profile reveals that AISI446 has a thicker oxide layer than austenite 349™, in addition AISI446 also has a higher ICR values than those of 349™ [15,16]. This indicates that the higher ICR values are due to a thicker film. Note that neither iron oxides nor chromium oxides dominate the composition of air-formed film on AISI446 steel. This is in excellent agreement with our previous investigation with 349™ steel [16], indicating that the air-formed oxide films formed on stainless steel are basically of the same composition, regardless the bulk structure of the steel. Assuming the half-height of the oxygen in oxide (O-oxide in Fig. 7) content as an estimate of the film/substrate steel interface [23], the air-formed film on ferrite AISI446 stainless steel requires approximately 3.5 min

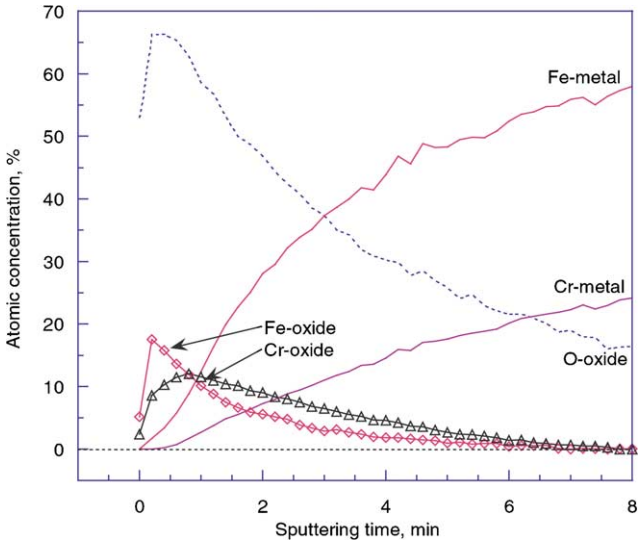

Fig. 7. XPS depth profile of fresh AISI446 stainless steel.

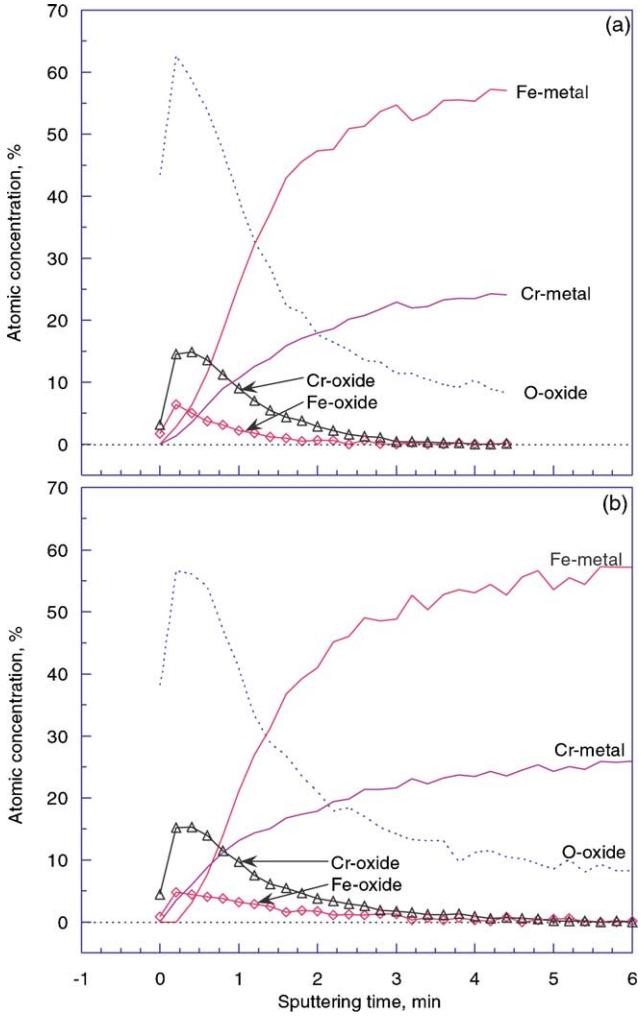

Fig. 8. XPS depth profile of AISI446 stainless steel polarized for 7.5 h in 1 M H_2SO_4 + 2 ppm F^- at 70 °C: (a) polarized at −0.1 V and the solution was purged with hydrogen gas; (b) polarized at 0.6 V and the solution was purged with air.

of sputtering, which is almost three times the time needed to sputter off the air-formed film on 349™ steel [18]. Adopting the sputtering rate of 20 Å/min, gives an estimate of the air-formed oxide film on AISI446 stainless steel as 7.0 nm, which is approximately three times the thickness of the air-formed film on austenite stainless steels [16,27,28].

The passive films are also composed of iron oxides and chromium oxide. However, in this case, chromium oxide dominates the passive film composition. Fig. 8 gives the depth profiles for AISI446 polarized both at −0.1 V in PEMFC anode environment (a) and at 0.6 V in simulated PEMFC cathode environment (b). It is seen that the surface composition depth profiles in Fig. 8a and b are identical to each other, indicating that the composition of the passive film formed is not affected by the applied potential and the purging gases. This is in agreement with the polarization behavior of the steel in simulated PEMFC environments, Figs. 1 and 2. Careful inspection of Fig. 8a and b shows that the depth profiles are slightly different. A longer time is needed to sputter off the oxides from the passive film formed in simulated PEMFC cathode environment (Fig. 8b) than the one formed in simulated PEMFC anode environment (Fig. 8a). AISI446 steel polarized in simulated PEMFC cathode environment has a deeper penetration depth of iron oxides and chromium oxide than that polarized in simulated PEMFC anode environment. In other words, AISI446 sample treated at 0.6 V (with air purge) has a thicker passive film than that treated at −0.1 V (with hydrogen purge). If we still use the half-height of the oxygen in oxide as the estimate of the film/substrate steel interface, the passive film treated at 0.6 V requires 1.5 min to sputter off, while the passive film treated at –0.1 V only requires 1.3 min to sputter off. This difference in sputtering times is directly related to the difference in film thickness. Adopting a sputtering rate of 20 Å/min, the passive film thickness is estimated to be 3.0 nm for AISI446 polarized at 0.6 V in simulated PEMFC cathode environment with air purge, and 2.6 nm for AISI446 polarized at −0.1 V in simulated PEMFC anode environment with hydrogen gas purge. These are identical to the passive film on 349™ under the same conditions [16], and are also in good agreement with passive films on other austenite stainless steels [27,29]. Thicker passive film then will give a higher value of interfacial contact resistance, as shown in Fig. 4. The XPS depth profile investigation correlates well with the ICR measurement.

4. Conclusions

Samples of AISI434, AISI436, AISI441, AISI444, and AISI446 ferrite stainless steels have been investigated in 1 M H_2SO_4 + 2 ppm F^- at 70 °C purged either with hydrogen gas or pressurized air to simulate a PEMFC bipolar plate environment. Both linear sweep voltammetry and interfacial contact resistance measurements indicated that the performance of the AISI446 stainless steel is superior to the others in this study.AISI446 showed very low critical and passivation currents in the solution purged either with hydrogen gas or with air. A stable passive film was formed within 20 min at −0.1 V in the solution sparged with hydrogen. However, it took 50 min to form a stable passive film at 0.6 V in the solution sparged with air. The ICR for AISI446 increased after passivation. XPS depth profiles indicate that air-formed surface film is composed of iron oxides and chromium oxide, neither dominates. The passive films on AISI446 are mainly chromium oxide, and the iron oxides play only a minor role. The passive film formed in the simulated PEMFC cathode environment is thicker than that formed in the simulated PEMFC anode environment, and the former resulted a higher interfacial contact resistance than the latter.

Acknowledgements

The authors wish to thank Georgia S. Machamer of J & L Specialty Steel, Inc. for the stainless steels samples. We are also indebted to Dr. Glenn Teeter for his assistance in the XPS investigation. This work was supported by the Hydrogen, Fuel Cells and Infrastructure Technologies Program of the US Department of Energy.

References

[1] B.C.H. Steele, A. Heinzel, Nature (Lond.) 414 (2001) 345.
[2] D. Busick, M. Wilson, in: D.H. Doughty, L.F. Nazar, M. Arakawa, H.-P. Brack, K. Naoi (Eds.), New Materials for Batteries and Fuel Cells: Mater. Res. Soc. Symp. Proc, vol. 575, Materials Research Society, USA, 2000, p. 247.
[3] J. Scholta, B. Rohland, V. Trapp, U. Focken, J. Power Sources 84 (1999) 231.
[4] O.J. Murphy, A. Cisar, E. Clarke, Electrochim. Acta 43 (1998) 3829.
[5] D.R. Hodgson, B. May, P.L. Adcock, D.P. Davies, J. Power Sources 96 (2001) 233.
[6] R. Hornung, G. Kappelt, J. Power Sources 72 (1998) 20.
[7] R.C. Makkus, A.H.H. Janssen, F.A. de Bruijn, R.K.A.M. Mallant, Fuel Cells Bull. 3 (2000) 5.
[8] R.C. Makkus, A.H.H. Janssen, F.A. de Bruijn, R.K.A.M. Mallant, J. Power Sources 86 (2000) 274.
[9] P.L. Hentall, J.B. Lakeman, G.O. Mepsted, P.L. Adcock, J.M. Moore, J. Power Sources 80 (1999) 235.
[10] D.P. Davies, P.L. Adcock, M. Turpin, S.J. Rowen, J. Power Sources 86 (2000) 237.
[11] D.P. Davies, P.L. Adcock, M. Turpin, S.J. Rowen, J. Appl. Electrochem. 30 (2000) 101.
[12] J. Scholta, B. Rohland, J. Garche, in: P.R. Roberge (Ed.), Proceedings of the 2nd International Symposium on New Materials for Fuel Cell and Modern Battery Systems, Ecole Polytechnique de Montreal, Canada, 1997, p. 300.
[13] M.S. Wilson, C. Zawodzinski, Fuel Cell with Metal Screen Flow Field, US Patent No. 6,037,072 (2000).
[14] S.J.C. Cleghorn, X. Ren, T. Espringer, M.S. Wilson, C. Zawodzinski, T.A. Zawodzinski, S. Gottesfeld, Int. J. Hydrogen Energy 22 (1997) 1137.
[15] H. Wang, M.A. Sweikart, J.A. Turner, J. Power Sources 5184 (2003) 1.
[16] H. Wang, J.A. Turner, J. Electrochem. Soc., Submitted for publication.

[17] J. Wind, R. Späh, W. Kaiser, G. Böhm, J. Power Sources 105 (2003) 256.
[18] L. Ma, S. Warthesen, D.A. Shores, J. New Mater. Electrochem. Syst. 3 (2000) 221.
[19] R.L. Borup, N.E. Vanderborgh, in: Proceedings of the Materials Research Society Symposium, vol. 393, Materials Research Society, USA, 1995, p. 151.
[20] L.L. Shreir, Corrosion, Vol. 2: Corrosion Control, second ed., Butterworths, London, UK, 1978, p. 11:113.
[21] M.G. Fontana, N.D. Greene, Corrosion Engineering, second ed., McGraw-Hill, New York, USA, 1978, p. 163.
[22] H.H. Uhlig, R.W. Revie, in: Corrosion and Corrosion Control: An Introduction to Corrosion Science and Engineering, third ed., Wiley, New York, USA, 1985, p. 78.
[23] M.Z. Yang, J.L. Luo, Q. Yang, L.J. Qiao, Z.Q. Qin, P.R. Norton, J. Electrochem. Soc. 146 (1999) 2107.
[24] P. Schmuki, S. Virtanen, A.J. Davenport, C.M. Vitus, J. Electrochem. Soc. 143 (1996) 3997.
[25] Y.F. Cheng, J.L. Luo, Electrochim. Acta 44 (1999) 4795.
[26] M.H.A. Elhamid, Y. Mikhail, in: G.J. Igwe, D. Mah (Eds.), Fuel cell technology: opportunities and challenges, 2002 AIChE Spring National Meeting, New Orleans, USA, 2002, p. 460.
[27] S. Bera, S. Rangarajan, S.V. Narasimhan, Corros. Sci. 42 (2000) 1709.
[28] P. Stefanov, D. Stoychev, M. Stoycheva, A.R. Gonzalez-Elipe, Ts. Marinova, Surf. Interface Anal. 28 (1999) 106.
[29] D. Wallinder, J. Pan, C. Leygraf, A. Delblanc-Bauer, Corros. Sci. 41 (1999) 275.